Author manuscript: Eur. Phys. J. D **76**(2), Art. Num. 32 (11 pages) (2022)

# Elliptic vector loci of average electron velocity of electron swarm in constant-collision-frequency model gas under ac electric and dc magnetic fields crossed at arbitrary angles*

**Hirotake Sugawara**[a,1], **Yuya Nakata**[1]

[1]Graduate School of Information Science and Technology, Hokkaido University, Sapporo 060-0814, Japan

**Abstract** The analytic solution of the average electron velocity vector $\mathbf{W}(t)$ of an electron swarm in gas under ac electric and dc magnetic fields ($\mathbf{E}(t)$ and $\mathbf{B}$, respectively) in a constant-collision-frequency model is extended to cover not only the known case of a right crossing angle ($\mathbf{E}(t) \perp \mathbf{B}$) but also the cases of arbitrary crossing angles ($\mathbf{E}(t) \not\perp \mathbf{B}$). The $x$, $y$, and $z$ components of $\mathbf{W}(t)$ are obtained as explicit formulae with the following parameters: the amplitude $E$ of $\mathbf{E}(t)$, the angle $\theta$ between $\mathbf{E}(t)$ and $\mathbf{B}$, the angular frequency $\omega_E$ of $\mathbf{E}(t)$, the cyclotron angular frequency $\omega_B$ (subject to the strength $B$ of $\mathbf{B}$), and the electron collision frequency $\nu$. A basic feature that $\mathbf{W}(t)$ draws elliptic locus in velocity space is unchanged even under $\mathbf{E}(t) \not\perp \mathbf{B}$, but the plane including the locus may tilt when $\omega_E$, $\omega_B$, or $\nu$ varies. The derivation of $\mathbf{W}(t)$ based on the analytic solution of single electron motion is detailed and fundamental behavior of the $\mathbf{W}(t)$ loci is observed to understand the electron transport under $\mathbf{E}(t) \times \mathbf{B}$ fields.

## 1 Introduction

Effects of magnetic fields on electrons in plasmas have been investigated as practical means of plasma control. For example, for negative ion sources [1], magnetic filter is typically used to suppress electron temperature [2–8], while contribution of local electron heating by electron cyclotron resonance (ECR) to production of negative ion precursor species is also suggested [9]. On the other hand, for material processing such as thin film deposition and etching, applicability of plasma parameter control by magnetic field is also suggested for dc discharges [10] and capacitively coupled plasmas [11]. Especially, for inductively coupled plasmas (ICPs), specific configurations of magnetic fields have been introduced expecting functional use of magnetic field; e.g. control of the plasma size and position [12], electron confinement for high plasma density [13–15], and plasma modulation for uniform wide-area processing and reduction of damage [13,15–17]. The electron heating in or near the plasma sheath under the Lorentz force [18–20] and the partial resonance [17,21] are also interesting phenomena that may contribute to efficient power deposition to magnetized plasmas for their sustainment.

On the other hand, the importance of compiling electron transport coefficients has been emphasized for reliable performance of plasma simulations [22,23]. For magnetized plasmas, especially for multi-dimensional fluid-model simulations under crossed electric and magnetic fields ($\mathbf{E} \times \mathbf{B}$ fields), direction-dependent data are demanded. In addition, the crossing angle $\theta$ between $\mathbf{E}$ and $\mathbf{B}$ extends the variation of the data needed. However, it is still rare even today that such data are available as a completed set. Necessity of some modification for non-magnetized transport coefficients is mentioned for simulations of magnetron plasmas [24], and electron transport coefficients in non-magnetized conditions are practically used as substitutes for those under $\mathbf{E} \times \mathbf{B}$ fields in modeling of ICPs for negative ion source [7] and device fabrication [25]. Hereafter, we let $\mathbf{E}$ and $\mathbf{B}$ denote dc electric and magnetic fields, respectively, and $\mathbf{E}(t)$ and $\mathbf{B}(t)$ do ac ones. Electron transport coefficients under $\mathbf{E} \perp \mathbf{B}$ have been analyzed since early

*Work supported by KAKENHI Grant JP19K03780 from the Japan Society for the Promotion of Science.
Published source: The European Physical Journal D, Volume 76, Issue 2, Article Number 32 (11 pages) (2022)
DOI: 10.1140/epjd/s10053-022-00346-1
[a]e-mail: sugawara@ist.hokudai.ac.jp

decades [26–32]. Efforts to analyze their $\theta$-dependence under $\mathbf{E} \not\perp \mathbf{B}$ have also been made vigorously [23,33–39]. Furthermore, temporally varying transport coefficients have been calculated for radio-frequency (rf) $\mathbf{E}(t) \perp \mathbf{B}(t)$ [40–44] and rf $\mathbf{E}(t) \not\perp \mathbf{B}(t)$ [45].

The present work focuses on the average electron velocity vector $\mathbf{W}(t)$ in periodic steady state under sinusoidal $\mathbf{E}(t)$ and constant $\mathbf{B}$. $\mathbf{W}(t)$ is regarded as a representative electron transport coefficient describing fundamental directionality of the electron flow. The present field configuration is typical in magnetized ICPs, where $\mathbf{B}(t)$ induced by the rf antenna current is treated to be negligibly smaller than $\mathbf{B}$ applied by the dc coil currents or permanent magnets. It was reported that $\mathbf{W}(t)$ in Ar, whose electron collision cross sections were taken from Ref. [46], draws elliptic vector loci under $\mathbf{E}(t) \perp \mathbf{B}$ [47]. The ellipse expands with increasing $|\mathbf{B}|$ up to around the ECR condition, and shrinks by the magnetic cooling effect under stronger $\mathbf{B}$. Its major axis deviates from the direction of $\mathbf{E}(t)$ monotonously with $|\mathbf{B}|$, which is considered to be an appearance of the Hall deflection. After this report, $\mathbf{W}(t)$ under $\mathbf{E}(t) \perp \mathbf{B}$ was derived analytically assuming that the electron collision frequency $\nu$ is constant and the electron scattering is isotropic [48,49]. The basic behavior of the elliptic vector locus observed in Ar was reproduced also in the constant-collision-frequency (CCF) model. This CCF model is much simpler than most of the real gases, but an example of real gas close to the CCF model to some extent has been reported [50,51]; an electron collision cross section set of $F_2$ [52,53] has an energy range in which the total collision frequency does not change significantly.

In this paper, we extend the CCF solution of $\mathbf{W}(t)$ to the cases of $\mathbf{E}(t) \not\perp \mathbf{B}$ [54], and the results are verified by Monte Carlo simulations as done in many preceding investigations. There are also some examples of multi-term Boltzmann equation analyses for the electron transport coefficients under $\mathbf{E} \perp \mathbf{B}$ [30,31], $\mathbf{E} \not\perp \mathbf{B}$ [23], $\mathbf{E}(t) \perp \mathbf{B}(t)$ [43], and $\mathbf{E}(t) \not\perp \mathbf{B}(t)$ [39]. However, publicly available simulation codes immediately applicable to the present verification are rarely found. Therefore, it would be an advantage that $\mathbf{W}(t)$ in the CCF model is described in an explicit form, because it enables us to predict fundamental dependence of the electron transport on the factors determining the $\mathbf{E}(t) \times \mathbf{B}$ fields. A CCF model gas is a characterless medium in the sense that the dependence of $\nu$ on the electron energy does not appear. Thus, the analytic solution of $\mathbf{W}(t)$ in the CCF model has a possibility to be a benchmark for characterizing the electron transport in real gases [51]. Details of the $\mathbf{W}(t)$ derivation are described, and some properties of $\mathbf{W}(t)$ in the CCF model are discussed on the basis of the formulae for the $x$, $y$, and $z$ components of $\mathbf{W}(t)$.

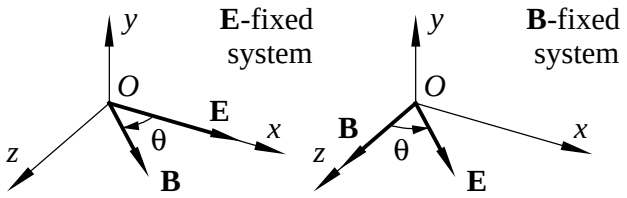


**Fig. 1** Coordinate systems. $\mathbf{E}$ is constant and ac electric field alternates as $\mathbf{E}(t) = \mathbf{E}\sin(\omega_E t + \phi)$

## 2 Model and conditions

### 2.1 Crossed ac electric and dc magnetic fields

Uniform $\mathbf{E}(t) = (E_x(t), E_y(t), E_z(t))$ and $\mathbf{B} = (B_x, B_y, B_z)$ are assumed in boundary-free space. $\mathbf{E}(t)$ is sinusoidal as $\mathbf{E}(t) = \mathbf{E}\sin(\omega_E t + \phi)$ and has a direction vector $\mathbf{E}$, an amplitude $E = |\mathbf{E}| > 0$, an ordinary frequency $f$, an angular frequency $\omega_E = 2\pi f$, and an initial phase $\phi$. $B = |\mathbf{B}| > 0$ is the strength of $\mathbf{B}$, and $\theta$ is the angle between $\mathbf{E}$ and $\mathbf{B}$.

For simplicity, we may fix either of $\mathbf{E}(t)$ and $\mathbf{B}$ in the $x$-, $y$- or $z$-direction without loss of generality. When $\mathbf{E}$ is fixed in the $x$-direction and $\mathbf{B}$ may vary with $\theta$ in the $xz$-plane,

$$\mathbf{E}(t) = (E\sin(\omega_E t + \phi), 0, 0), \tag{1}$$

$$\mathbf{B} = (B\cos\theta, 0, B\sin\theta). \tag{2}$$

On the other hand, when $\mathbf{B}$ is fixed in the $z$-direction and $\mathbf{E}$ may vary with $\theta$ in the $xz$-plane,

$$\mathbf{E}(t) = (E\sin\theta\sin(\omega_E t + \phi), 0, E\cos\theta\sin(\omega_E t + \phi)), \tag{3}$$

$$\mathbf{B} = (0, 0, B). \tag{4}$$

These arrangements are shown in Figure 1. Let us call them the $\mathbf{E}$-fixed and the $\mathbf{B}$-fixed systems, respectively. When we distinguish vectors in these systems, the vectors and their components are denoted with superscripts $\mathbf{E}$ and $\mathbf{B}$ as $\mathbf{r}^{\mathbf{E}} = (x^{\mathbf{E}}, y^{\mathbf{E}}, z^{\mathbf{E}})$ and $\mathbf{r}^{\mathbf{B}} = (x^{\mathbf{B}}, y^{\mathbf{B}}, z^{\mathbf{B}})$, respectively. Any given vector is convertible between these systems by the relations presented in Appendix A.

### 2.2 Single electron motion

The equation of motion for electron velocity $\mathbf{v}(t) = (v_x(t), v_y(t), v_z(t))$ under $\mathbf{E}(t)$ and $\mathbf{B}$ is

$$\frac{\mathrm{d}}{\mathrm{d}t}\mathbf{v}(t) = -\frac{e}{m}\left(\mathbf{E}(t) + \mathbf{v}(t) \times \mathbf{B}\right), \tag{5}$$

where $e$ and $m$ are the electronic charge and mass, respectively. Analytic solutions of $\mathbf{v}(t)$ under $\mathbf{E}(t) \not\perp \mathbf{B}$ are presented in Appendix B and Appendix C. There are two sets of solutions corresponding to the ECR condition $\omega_E = \omega_B$ and non-ECR condition $\omega_E \neq \omega_B$. Here, the $B$ value satisfying the ECR condition is the resonant magnetic field strength $B_{\mathrm{ECR}} = 2\pi(m/e)f$, and $B_{\mathrm{ECR}} = 0.4844\,\mathrm{mT}$ at a typical radio frequency $f = 13.56\,\mathrm{MHz}$.

It is seen that the solutions in the **B**-fixed system are simpler than in the **E**-fixed system. Therefore, the description is hereafter based on the formulae in the **B**-fixed system.

### 2.3 Electron–molecule interactions

The gas medium is assumed to have such electron collision cross sections $q_k(\varepsilon)$ that the total collision frequency $\nu = Nq_{\mathrm{total}}(\varepsilon)v$ is constant; i.e.

$$q_{\mathrm{total}}(\varepsilon) = \sum_k q_k(\varepsilon) \propto \frac{1}{v} \propto \frac{1}{\sqrt{\varepsilon}}, \tag{6}$$

where $v = |\mathbf{v}|$ is electron speed, $\varepsilon = \frac{1}{2}mv^2$ is electron energy, $N$ is gas molecule number density, $q_k(\varepsilon)$ is the collision cross section of the $k$th kind of electron–molecule interaction as a function of $\varepsilon$, and $q_{\mathrm{total}}(\varepsilon)$ is the sum of $q_k(\varepsilon)$. It is assumed that the electron scattering by each collisional process is isotropic in the laboratory coordinate system.

The CCF condition is known as a result of an induced dipole model. However, real gases do not necessarily fit the CCF model, especially in case the $\varepsilon$-dependence of $q_{\mathrm{total}}$ is complicated in the presence of inelastic processes with thresholds. A rough prospect for the CCF feature of a gas could be given by observing the variation width of $Nq_{\mathrm{total}}v$ for the gas in a main range of $\varepsilon$ to which the majority of electrons in the swarm belong [51].

### 2.4 Definition of electron transport coefficients

We consider the average electron velocity vector $\mathbf{W}(t) = \langle \mathbf{v}(t) \rangle$ of an electron swarm under $\mathbf{E}(t)$ and $\mathbf{B}$:

$$\begin{aligned} \mathbf{W}(t) &= (W_x(t), W_y(t), W_z(t)) \\ &= (\langle v_x(t) \rangle, \langle v_y(t) \rangle, \langle v_z(t) \rangle), \end{aligned} \tag{7}$$

where $\langle x \rangle$ represents the ensemble average of a quantity $x$ over the electron swarm. If an electron velocity distribution function (EVDF) $f(\mathbf{v}, t)$ is given, a component $W_*(t)$ of $\mathbf{W}(t)$ ('$*$' represents one of $x$, $y$, and $z$) is obtained as

$$W_*(t) = \left[ \int_{\mathbf{v}} v_* f(\mathbf{v}, t) \mathrm{d}\mathbf{v} \right] / \left[ \int_{\mathbf{v}} f(\mathbf{v}, t) \mathrm{d}\mathbf{v} \right]. \tag{8}$$

As well, in Monte Carlo simulations, $W_*(t)$ is obtained by sampling $v_*(t)$ as

$$W_*(t) = \frac{1}{n(t)} \sum_{i=1}^{n(t)} v_{*,i}(t), \tag{9}$$

where $v_{*,i}(t)$ is $v_x(t)$, $v_y(t)$, or $v_z(t)$ of the $i$th electron in the swarm consisting of $n(t)$ electrons.

In periodic steady state, $n(t)$ in the presence of electron increase due to ionization and/or decrease due to electron attachment is assumed to develop exponentially every ac period $T = 1/f$ as

$$n(t + T) = n(t) \exp(\bar{\nu}_{\mathrm{ion},T} T). \tag{10}$$

Here, the periodic steady state refers to a condition under which an electron transport coefficient $p$ satisfies $p(t + T) = p(t)$ (not necessarily sinusoidal), and $\bar{\nu}_{\mathrm{ion},T}$ is time-averaged effective ionization frequency defined with those for ionization and electron attachment as $\bar{\nu}_{\mathrm{ion},T} = \nu_{\mathrm{ion},T} - \nu_{\mathrm{att},T}$. Note that the instantaneous values of the ionization and electron attachment frequencies, $\nu_{\mathrm{ion}}(t)$ and $\nu_{\mathrm{att}}(t)$, respectively, may vary with the periodic variation of the EVDF of the electron swarm. The CCF condition does not guarantee constant $\nu_{\mathrm{ion}}(t)$ and $\nu_{\mathrm{att}}(t)$. Therefore, an electron-conservative case $\nu_{\mathrm{ion}}(t) = \nu_{\mathrm{att}}(t) = 0$, thus $\bar{\nu}_{\mathrm{ion},T} = 0$, is assumed in the beginning as the most basic case in the derivation of $\mathbf{W}(t)$. An approximation in the electron-nonconservative case is mentioned afterward.

## 3 Derivation of $\mathbf{W}(t)$

### 3.1 Outline

A concept of electron swarm subsets that compose the whole electron swarm is introduced to calculate $\mathbf{W}(t)$. A subset consists of the electrons starting their free flight together by scattering during a common period $\mathrm{d}t'$ in $t' \leq t \leq t' + \mathrm{d}t'$. These electrons belong to the subset during collisionless free flight. The electrons scattered by gas molecules quit the subset and make a new subset together with those scattered out of the other subsets at the same time (see Fig. 2).

$\mathbf{W}(t)$ is obtained by integrating the average electron velocity of a subset weighted by the electron population of the subset. Here, we utilize a feature that the average electron velocity of a subset varies in the same way as the single electron motion starting from $\mathbf{v} = 0$ at $t = t'$. This approach has been adopted for electron swarms under $\mathbf{E} \perp \mathbf{B}$ [50] and $\mathbf{E}(t) \perp \mathbf{B}$ [48], and is applicable also to the present condition $\mathbf{E}(t) \not\perp \mathbf{B}$ as elucidated below.

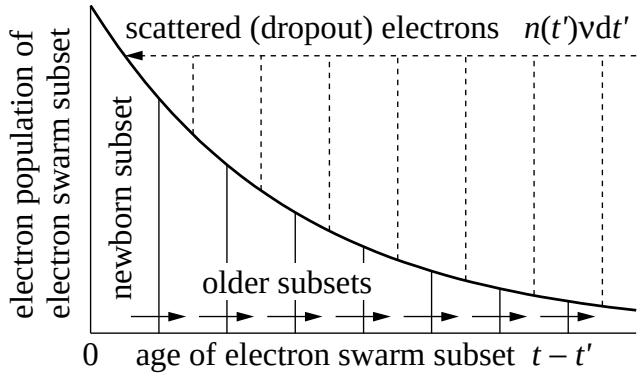


**Fig. 2** Schematic of electron swarm subsets

### 3.2 Behaviour of electron swarm subset

First, for the assumption of isotropic scattering, the initial value $\langle \mathbf{v}(t') \rangle$ of the electrons belonging to a newborn subset is zero; any $\mathbf{v}$ of an electron is canceled by its counterpart having $-\mathbf{v}$. At $t = t'$, the EVDF of the newborn subset is isotropic around the origin $\mathbf{v} = 0$ of velocity space.

Next, the EVDF of the subset remains isotropic around the $\mathbf{v}(t)$ of the moving center of the subset during free flight. In the $\mathbf{B}$-fixed system, the acceleration acting on the electrons induces their rotational displacement in velocity space around a common axis

$$v_x = 0, \quad v_y = -\frac{E}{B}\sin\theta\sin(\omega_E t + \phi) \quad \text{for all } v_z \tag{11}$$

parallel to the $v_z$-axis (the direction of $\mathbf{B}$) with a common angular frequency $\omega_B$ as shown in Appendix D. Then, the motion of the center of the subset is still identical to that of a single electron starting from $\mathbf{v} = 0$, because the center of the subset moves in the same rotation.

Furthermore, the isotropy of the EVDF of the subset is kept even in the presence of scattering. Electrons may dropout from the subset by scattering but the dropout electrons appear in proportion to the EVDF of the subset because the scattering is equiprobable for all electrons under constant $\nu$. The EVDF of the subset decays exponentially keeping its shape similar to its initial distribution.

### 3.3 Weight of electron population

Let $\mathrm{d}n(t)$ be the electron population of a subset produced in a short period $t' \le t \le t' + \mathrm{d}t'$. Its initial value is $\mathrm{d}n(t') = n(t')\nu\mathrm{d}t'$, where $n(t')$ is the electron population of the whole electron swarm at $t = t'$. Under the CCF condition, $\mathrm{d}n(t)$ decays exponentially with time as

$$\mathrm{d}n(t) = n(t')\nu\mathrm{d}t' \exp[-\nu(t - t')]. \tag{12}$$

The weight of the subset in the whole electron swarm is $\mathrm{d}n(t)/n(t)$.

### 3.4 Derivation of $\mathbf{W}(t)$ from single electron motion

$\mathbf{W}(t)$ is derived from the analytic solution of $\mathbf{v}(t)$ for single electron motion under $\mathbf{E}(t)\times\mathbf{B}$. $\mathbf{W}(t)$ is obtained by integrating $\mathbf{v}(t)$ of the center of each subset with its weight:

$$\mathbf{W}(t) = \frac{1}{n(t)}\int_{-\infty}^{t} \mathbf{v}(t - t')\exp[-\nu(t - t')]n(t')\nu\mathrm{d}t' \tag{13}$$

Here, $\mathbf{v}(t-t')$ is substituted by the analytic solution of single electron motion $\mathbf{v}^{\mathbf{B}}(t-t')$ shown in Appendix B with an initial condition $(v^{\mathbf{B}}_{x0}, v^{\mathbf{B}}_{y0}, v^{\mathbf{B}}_{z0}) = (0, 0, 0)$. [1]

The solution of $\mathbf{W}^{\mathbf{B}}(t)$ is obtained as follows: [2]

$$W^{\mathbf{B}}_x(t) = v_E\sin\theta\frac{\omega_E^2(\omega_E^2 - \omega_B^2 + \nu^2)\cos(\omega_E t + \phi)}{[(\omega_E - \omega_B)^2 + \nu^2]\,[(\omega_E + \omega_B)^2 + \nu^2]} - v_E\sin\theta\frac{\nu\omega_E(\omega_E^2 + \omega_B^2 + \nu^2)\sin(\omega_E t + \phi)}{[(\omega_E - \omega_B)^2 + \nu^2]\,[(\omega_E + \omega_B)^2 + \nu^2]}, \tag{14}$$

$$W^{\mathbf{B}}_y(t) = v_E\sin\theta\frac{2\nu\omega_E^2\omega_B\cos(\omega_E t + \phi)}{[(\omega_E - \omega_B)^2 + \nu^2]\,[(\omega_E + \omega_B)^2 + \nu^2]} + v_E\sin\theta\frac{\omega_E\omega_B(\omega_E^2 - \omega_B^2 - \nu^2)\sin(\omega_E t + \phi)}{[(\omega_E - \omega_B)^2 + \nu^2]\,[(\omega_E + \omega_B)^2 + \nu^2]}, \tag{15}$$

$$W^{\mathbf{B}}_z(t) = v_E\cos\theta\frac{\omega_E^2}{\omega_E^2 + \nu^2}\cos(\omega_E t + \phi) - v_E\cos\theta\frac{\nu\omega_E}{\omega_E^2 + \nu^2}\sin(\omega_E t + \phi), \tag{16}$$

$$v_E = \frac{eE}{m\omega_E}, \tag{17}$$

where $v_E$ is a specific electron speed under a sinusoidal ac $\mathbf{E}(t)$ in the absence of $\mathbf{B}$; i.e. the amplitude of the $\mathbf{v}(t)$ component parallel to $\mathbf{E}(t)$ in collisionless free flight. This $\mathbf{W}(t)$ solution is common for the non-ECR and the ECR cases. $W^{\mathbf{B}}_x(t)$ and $W^{\mathbf{B}}_y(t)$ at $\theta = \pi/2$ agree with the results under $\mathbf{E}(t) \perp \mathbf{B}$ presented in preceding reports [48,49,51], in which $W^{\mathbf{B}}_z(t) = 0$.

[1] At this substitution, the initial phase $\phi$ in the solution of $\mathbf{v}^{\mathbf{B}}(t)$ becomes $\omega_E t' + \phi$. However, the appearance of factors $\sin(\omega_E t + \phi)$ and $\cos(\omega_E t + \phi)$ in the components of $\mathbf{v}^{\mathbf{B}}(t)$ in the integrand are unchanged because $t$ and $\phi$ in $\omega_E t + \phi$ are replaced by $(t - t')$ and $(\omega_E t' + \phi)$, respectively, as $\omega_E(t - t') + (\omega_E t' + \phi)$ and this returns to $\omega_E t + \phi$.

[2] All terms include a common factor $\omega_E$, which may cancel with that included in $v_E$; $v_E\omega_E$ is the amplitude of the electron acceleration as it has been denoted as $a$ in Ref. [49].

All of $W_x^{\mathbf{B}}(t)$, $W_y^{\mathbf{B}}(t)$, and $W_z^{\mathbf{B}}(t)$ consist of terms of $\sin(\omega_E t+\phi)$ and $\cos(\omega_E t+\phi)$. This represents that the vector head of $\mathbf{W}(t)$ draws an elliptic locus periodically with $t$. The solution represented in the $\mathbf{E}$-fixed system is obtained by the conversion with the relations in (A.2), but the conversion makes the formulae more complicated.

## 4 Discussion

### 4.1 Verification of theory by Monte Carlo simulation

The theoretical results are verified by Monte Carlo simulations for electron swarms in a CCF model gas, which is slightly modified from its original definition [55]. The gas has the cross section of elastic collision $q_{\mathrm{el}}$ and those of inelastic collisions $q_{\mathrm{inel},1}$ and $q_{\mathrm{inel},2}$ with thresholds 10 and 15 eV, respectively. Their quantitative definition is detailed in Appendix E. In the examination of the electron-conservative case, $q_{\mathrm{inel},1}$ and $q_{\mathrm{inel},2}$ are treated as excitation cross sections.

$\mathbf{E}(t)$ was set as $E = 2.0\,\mathrm{V\,cm^{-1}}$, $f = 13.56\,\mathrm{MHz}$, and $\phi = 0$. $B$ was fixed at $B_{\mathrm{ECR}} = 0.4844\,\mathrm{mT}$. $\nu$ was set at $4.0\times10^7\,\mathrm{s^{-1}}$. In the present CCF model gas, this $\nu$ value corresponds to $N = 1.69\times10^{20}\,\mathrm{m^{-3}}$ (0.698 Pa or 5.25 mTorr at 300 K), which is in a typical condition range of magnetized plasmas. The values of reduced electric and magnetic fields are, respectively, $E/N = 1180\,\mathrm{Td}$ (1 Td (townsend) $= 10^{-21}\,\mathrm{V\,m^2}$) and $B/N = 2860\,\mathrm{Hx}$ (1 Hx (huxley) $= 10^{-27}\,\mathrm{T\,m^3}$).

The initial $\mathbf{v}$ of electrons were chosen at random from a Maxwellian EVDF with a mean electron energy of 1 eV. Flights of $10^6$ electrons were traced for $50T$, within which $\mathbf{W}(t)$ reached its periodic steady state, using the Runge–Kutta method with a time step $\Delta t = T/24\,000 = 3.07\,\mathrm{ps}$, where $T = 73.7\,\mathrm{ns}$. Instead of the analytic solutions (14)-(16), the equations of motion obtained by discretizing (5) for $\Delta t$ were calculated to obtain independent results for verification. The $\mathbf{W}(t)$ values were obtained as the phase-resolved averages in the final $5T$ for every $T/24$ or $\pi/12$.

Figure 3 shows the elliptic vector loci for $0 \le \theta \le \pi/2$. The agreement of the results between the theory and the Monte Carlo simulations verifies that the analytic solution of $\mathbf{W}(t)$ is appropriate.

### 4.2 Dependence of $\mathbf{W}(t)$ on the parameters

Compared with a specific case $\theta = \pi/2$ presented in [48, 49,51], it is seen in (14)–(16) that $W_x^{\mathbf{B}}(t)$ and $W_y^{\mathbf{B}}(t)$ have the same dependence on the parameters except for an additional factor $\sin\theta$ and that $W_z^{\mathbf{B}}(t)$ becomes

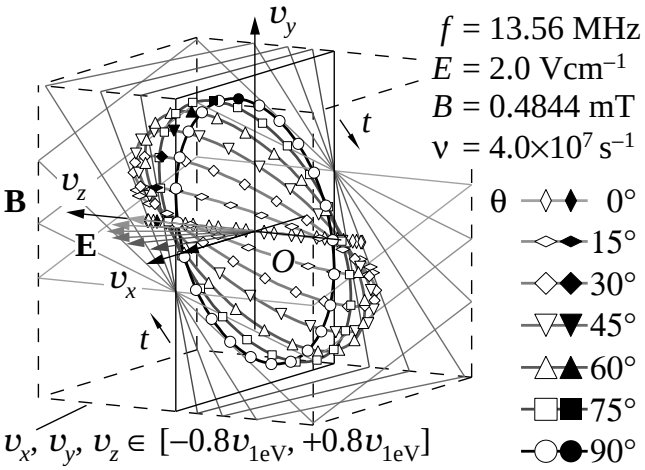


**Fig. 3** $\mathbf{W}(t)$ and its elliptic vector loci in periodic steady state at various $\theta$ values in the electron-conservative case. Solid curves, theory; and symbols, Monte Carlo simulation for every $\pi/12$ of the $\mathbf{E}(t)$ phase. The full symbols represent the $\mathbf{W}(t)$ values at phases of $\omega_E t = 2n\pi$ ($n$ is an integer). The vector head of $\mathbf{W}(t)$ draws an ellipse with $t$ clockwise in this view. The dashed lines indicate a cubic region of $|v_*| \le 0.8v_{1\mathrm{eV}}$ ($v_*$: $v_x$, $v_y$, and $v_z$), where $v_{1\mathrm{eV}}$ is the electron speed associated with 1 eV. The parallelograms are the intersections between the cube and the vector planes including the elliptic vector loci

non-zero with a factor of $\cos\theta$ for $\theta \ne \pi/2$. $\mathbf{W}_z^{\mathbf{B}}(t)$ is essentially independent of $\omega_B$. The periodic response of $\mathbf{W}^{\mathbf{B}}(t)$ in the $\mathbf{B}$ direction is induced purely by $E_z^{\mathbf{B}}(t)$. It is common for $\mathbf{W}_x^{\mathbf{B}}(t)$, $\mathbf{W}_y^{\mathbf{B}}(t)$, and $\mathbf{W}_z^{\mathbf{B}}(t)$ that the amplitude is proportional to $E$.

$\nu$ is the only medium-origin parameter, while the others are the parameters determining the field arrangement. The CCF model ignores the temporal variation of $\nu$ which would occur in real gases. Thus, under $\mathbf{E}(t) \not\perp \mathbf{B}$ as well, characteristics of $\mathbf{W}(t)$ in a real gas originating in its electron collision cross sections would appear in the deviation of $\mathbf{W}(t)$ from the elliptic vector loci predicted by the CCF model through $\nu$ as demonstrated under $\mathbf{E}(t) \perp \mathbf{B}$ [51].

### 4.3 Vector plane

There exists such a plane (say vector plane), $N_x^{\mathbf{B}}v_x + N_y^{\mathbf{B}}v_y + N_z^{\mathbf{B}}v_z = 0$, that includes an elliptic vector locus of $\mathbf{W}^{\mathbf{B}}(t)$ and the origin of velocity space. Its normal vector $\mathbf{N}^{\mathbf{B}} = (N_x^{\mathbf{B}}, N_y^{\mathbf{B}}, N_z^{\mathbf{B}})$ satisfies $\mathbf{W}^{\mathbf{B}}(t) \perp \mathbf{N}^{\mathbf{B}}$, thus $\mathbf{W}^{\mathbf{B}}(t)\cdot\mathbf{N}^{\mathbf{B}} = 0$. An example $\mathbf{N}^{\mathbf{B}}$ (not a unit vector) is

$$\mathbf{N}^{\mathbf{B}} = ((\omega_E^2 - \omega_B^2 + \nu^2)\cos\theta, 2\nu\omega_B\cos\theta, -(\omega_E^2 + \nu^2)\sin\theta). \tag{18}$$

The vector plane may turn when a parameter in (18) varies. Figure 3 shows the turn of the vector plane with

$\theta$. Because $N_x^{\mathbf{B}}$ and $N_y^{\mathbf{B}}$ have a common factor $\cos\theta$, the turn has a fixed axis represented as

$$v_y = -\frac{\omega_E^2 - \omega_B^2 + \nu^2}{2\nu\omega_B} v_x, \quad v_z = 0. \tag{19}$$

Such a fixed axis associated with a single parameter is not found in the **E**-fixed system; the $\mathbf{N}^{\mathbf{E}}$ corresponding to $\mathbf{N}^{\mathbf{B}}$ in (18) is

$$\mathbf{N}^{\mathbf{E}} = (-\omega_B^2 \sin\theta\cos\theta, 2\nu\omega_B\cos\theta, -(\omega_E^2 + \nu^2) + \omega_B^2\cos^2\theta). \tag{20}$$

### 4.4 Axes of elliptic vector loci

The direction of the major axis of the ellipse is considered to represent that of the average Hall deflection [48,51]. The lengths $L_+$ and $L_-$ of the semi-major and semi-minor axes, respectively, represent the sensitivity of the $\mathbf{W}(t)$ response along and perpendicular to the direction of the Hall deflection. $L_+$ and $L_-$ satisfy

$$L_\pm^2 = \frac{1}{2}v_E^2\omega_E^2\left[\frac{(\omega_E^2 + \omega_B^2 + \nu^2)\sin^2\theta}{\Omega} + \frac{\cos^2\theta}{\Xi}\right] \pm \frac{1}{2}v_E^2\omega_E^2\sqrt{\frac{\sin^2\theta}{\Omega} - \frac{\omega_B^4\sin^2\theta\cos^2\theta}{\Omega\Xi^2} + \frac{\cos^2\theta}{\Xi^2}}, \tag{21}$$

$$\Omega = \left[(\omega_E - \omega_B)^2 + \nu^2\right]\left[(\omega_E + \omega_B)^2 + \nu^2\right], \tag{22}$$

$$\Xi = \omega_E^2 + \nu^2. \tag{23}$$

The vertices of an elliptic vector locus are obtained by giving the following conditions to (14)–(16):

$$(\cos(\omega_E t + \phi), \sin(\omega_E t + \phi)) = \left(\pm\tfrac{1}{2}\sqrt{1+X} \pm \tfrac{1}{2}\sqrt{1-X}, \pm\tfrac{1}{2}\sqrt{1+X} \mp \tfrac{1}{2}\sqrt{1-X}\right), \tag{24}$$

$$X = -2\nu\omega_E\left(\frac{\sin^2\theta}{\Omega} + \frac{\cos^2\theta}{\Xi^2}\right) \times \left(\frac{\sin^2\theta}{\Omega} - \frac{\omega_B^4\sin^2\theta\cos^2\theta}{\Omega\Xi^2} + \frac{\cos^2\theta}{\Xi^2}\right)^{-1/2}. \tag{25}$$

Their derivation is presented in Appendix F.

### 4.5 Effects of ionization and electron attachment

Ionization increases the portion of the isotropically distributing electrons in the EVDF by adding secondary electrons to the swarm. This results in decrease of the directionality of the whole electron swarm. On the other hand, electron attachment reduces the population of scattered electrons. The elliptic vector locus shrinks by ionization and swells by attachment.

It is mentioned in Ref. [48] for $\mathbf{E}(t) \perp \mathbf{B}$ that the solution in the presence of ionization and/or electron attachment has such a form in which $\nu$ is replaced with $\nu + \bar{\nu}_{\rm ion}$, where $\bar{\nu}_{\rm ion}$ is regarded to be constant in the theory. A factor $n(t')(\nu + \bar{\nu}_{\rm ion})\mathrm{d}t'$ represents the initial population or weight of the electron swarm subset consisting of the electrons scattered in $\mathrm{d}t'$. This applies also to the case $\bar{\nu}_{\rm ion} < 0$, in which electron attachment is dominant. Here, $\nu$ is constant under the CCF assumption and dependent only on the characteristics of the gas, but $\bar{\nu}_{\rm ion}$ may vary temporally depending on the EVDF. Therefore, time-averaged values of $\nu + \bar{\nu}_{\rm ion}$ is substituted for $\nu$ in (14)–(16) as an approximation for $\mathbf{W}(t)$ in electron-nonconservative cases. This treatment gave reasonable estimations for $\mathbf{W}(t)$ under $\mathbf{E}(t) \perp \mathbf{B}$ in a real gas $F_2$ in comparisons with results of Monte Carlo simulations [51].

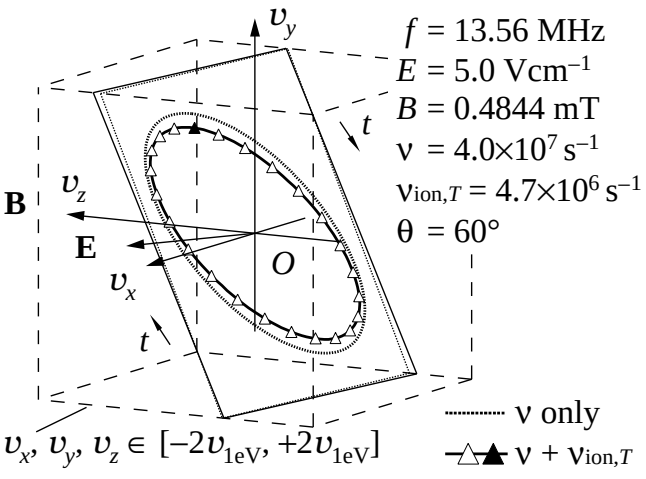


**Fig. 4** Elliptic vector locus under the influence of ionization. Solid and dotted curves, theory; triangles, Monte Carlo simulation for every $\pi/12$ of the $\mathbf{E}(t)$ phase. The full triangle represents the $\mathbf{W}(t)$ value at phases of $\omega_E t = 2n\pi$ ($n$ is an integer)

In the present work for $\mathbf{E}(t) \not\perp \mathbf{B}$, as well, the applicability of the substitution of $\nu + \bar{\nu}_{\rm ion}$ for $\nu$ is demonstrated. Figure 4 shows the result of a Monte Carlo simulation performed at $E = 5.0\,\mathrm{V\,cm^{-1}}$ ($E/N = 2960\,\mathrm{Td}$), $f = 13.56\,\mathrm{MHz}$, $\phi = 0$, $B = 0.4844\,\mathrm{mT}$, and $\theta = \pi/3$ treating $q_{\rm inel,2}$ of the CCF model gas as ionization cross section. Here, $n(t)$ in (9) includes the secondary electrons. The time-averaged $\nu_{\rm ion}(t)$ value, $\nu_{{\rm ion},T} = \bar{\nu}_{{\rm ion},T}$, which is substituted for $\bar{\nu}_{\rm ion}$ in the theory, becomes about 12% of $\nu$ in the present condition. This amount of $\nu_{{\rm ion},T}$ induces a recognizable difference. Equations (14)–(16) not taking $\nu_{{\rm ion},T}$ into account overestimate the components of $\mathbf{W}(t)$ and the elliptic vector locus is larger than the Monte Carlo results. However, the substitution of $\nu + \nu_{{\rm ion},T}$ for $\nu$ gives a fine approximation for the Monte Carlo results.

In addition to the size change of the elliptic vector locus, the electron-nonconservative effect induces a turn of the vector plane. This is because its normal vector

includes $\nu$ (to be replaced with $\nu + \nu_{\mathrm{ion},T}$) as a factor not proportional between $N_x$, $N_y$, and $N_z$.

### 4.6 Affinity of formulation with coordinate system

Many preceding investigations under $\mathbf{E} \not\perp \mathbf{B}$ [33–36] and $\mathbf{E}(t) \not\perp \mathbf{B}(t)$ [40,45] employ the **E**-fixed system. The **E**-fixed system is convenient in focusing on the electron transport in the direction of the motive force, for example, concerned with the electron energy increase and decrease. On the other hand, the simplicity of the solutions of $\mathbf{v}(t)$ and $\mathbf{W}(t)$ under $\mathbf{E}(t) \not\perp \mathbf{B}$ is an advantage of the **B**-fixed system. Electrons are transported basically along magnetic flux lines and the action of the applied electric field can easily be separated into the components parallel and perpendicular to **B**. The presence of the fixed axis for the turn of the vector plane pointed out in section 4.3 also suggests the affinity of the **B**-fixed system with analyses of the electron transport under $\mathbf{E}(t) \not\perp \mathbf{B}$.

### 4.7 Possibility of extension to other field conditions

$\mathbf{W}(t)$ in the CCF condition can be calculated by (13) even under $\mathbf{E}(t) \times \mathbf{B}(t)$ as long as $\mathbf{E}(t)$ and $\mathbf{B}(t)$ are position-independent and $n(t)$ of the whole electron swarm and $\mathbf{v}(t-t')$ of the single electron motion are available. When the analytic solution of $\mathbf{v}(t-t')$ under the given $\mathbf{E}(t) \times \mathbf{B}(t)$ is not available, (13) is to be calculated by solving $\mathbf{v}(t-t')$ step by step for every $\Delta t$ numerically. Typical cases are, for example, sinusoidal $\mathbf{E}(t)$ and $\mathbf{B}(t)$ which model electromagnetic induction (when phase difference is $\pi/2$ [40–42,44,45]) and electromagnetic wave (when synchronous and $\mathbf{E}(t) \perp \mathbf{B}(t)$), and non-sinusoidal $\mathbf{E}(t)$ as is for impulse-driven plasmas.

It would be convenient to use arrays to store the $x$, $y$, and $y$ components of $\mathbf{v}(t-t')$; the solution of $\mathbf{v}(t-t')$ may differ depending on $t'$, the birth time of electron swarm subset, because the initial conditions $\mathbf{E}(t')$ and $\mathbf{B}(t')$ for each subset vary temporally. The required size of the arrays is $n_{\Delta t} = t_{\max}/\Delta t$, where $t_{\max}$ is the maximum length of the integration domain $[t', t]$; $t_{\max} = (t-t')|_{\max}$. It is necessary to choose a finite but sufficiently long $t_{\max}$ to terminate the integration back to $t' = -\infty$ at an acceptable convergence under the exponential decay of the weight $\exp[-\nu(t-t')]$.

The computational load would be proportional to $n_{\Delta t}^2$ for 1 through $n_{\Delta t}$ steps of temporal variation of $\mathbf{v}(t-t')$ of $n_{\Delta t}$ subsets. [3] In case we need the temporal variation of $\mathbf{W}(t)$ for a period $T$, as is in case $\mathbf{E}(t)$ and $\mathbf{B}(t)$ are periodic functions, it is obtained by shifting $t$ for $T/\Delta t$ steps. The load of this calculation is also proportional to $n_{\Delta t}^2$ when $t_{\max}$ is chosen to be proportional to $T$.

[3] To obtain $\mathbf{v}(t)$, only one step is necessary for the newborn subset, and $n_{\Delta t}$ steps are needed for the oldest subset.

## 5 Conclusion

Formulae for the periodic response of the average electron velocity vector $\mathbf{W}(t)$ of an electron swarm under ac $\mathbf{E}(t)$ and dc $\mathbf{B}$ fields crossed at arbitrary angles $\theta$ have been derived analytically from the solution of velocity $\mathbf{v}(t)$ for single electron motion, under the assumptions of a CCF condition and isotropic scattering. This work is an extension of the formulae from the system under $\mathbf{E}(t) \perp \mathbf{B}$ to that under $\mathbf{E}(t) \not\perp \mathbf{B}$. The validity of the formulae has been verified with results of Monte Carlo simulations using a CCF model gas, which agree well with the theoretical prediction.

$\mathbf{W}(t)$ draws periodically an elliptic locus in a vector plane under given $E$, $\omega_E$, $\omega_B$ (subject to $B$), $\theta$, and $\nu$ (or $\nu + \bar{\nu}_{\mathrm{ion},T}$). The normal vector of the vector plane indicates that the plane may tilt depending on $\omega_E$, $\omega_B$, $\nu$, and $\theta$ unlike the case under $\mathbf{E}(t) \perp \mathbf{B}$. At that time, the major axis of the ecliptic vector locus, which is considered to represent the direction of the Hall deflection, is also slanted with a complicated dependence on the parameters. In addition, an electron-nonconservative case in the presence of the secondary electron supply due to ionization has been examined and it has been demonstrated that the approximation adopted in the theory reasonably reflects the influence of ionization.

It is beneficial that fundamental dependence of $\mathbf{W}(t)$ on $E$, $\omega_E$, $\omega_B$, $\theta$, and $\nu$ is explicitly shown in the formulae. Even in case the electron transport coefficients in the gas medium are not compiled well, investigators can have an approximated overview of the ac response of directional electron flow under a given $\mathbf{E}(t) \times \mathbf{B}$ fields by assuming a $\nu$ value. This would assist insight of investigators and reasonable fluid modeling of magnetized plasmas.

**Acknowledgements** This work was supported by KAKENHI Grant No. JP19K03780 from the Japan Society for the Promotion of Science.

## Appendix A: Coordinate conversion between the E-fixed and the B-fixed systems

When vectors $(x^{\mathbf{E}}, y^{\mathbf{E}}, z^{\mathbf{E}})$ in the **E**-fixed system and $(x^{\mathbf{B}}, y^{\mathbf{B}}, z^{\mathbf{B}})$ in the **B**-fixed system are equivalent to each other with respect to the direction relative to **E**

and **B**, the components of one can be obtained from those of the other by the following relations representing rotations around the $y$-axis by angles $\pm(\pi/2-\theta)$:

$$\begin{cases} x^{\mathbf{B}} = x^{\mathbf{E}}\sin\theta - z^{\mathbf{E}}\cos\theta \\ y^{\mathbf{B}} = y^{\mathbf{E}} \\ z^{\mathbf{B}} = x^{\mathbf{E}}\cos\theta + z^{\mathbf{E}}\sin\theta \end{cases}, \tag{A.1}$$

$$\begin{cases} x^{\mathbf{E}} = x^{\mathbf{B}}\sin\theta + z^{\mathbf{B}}\cos\theta \\ y^{\mathbf{E}} = y^{\mathbf{B}} \\ z^{\mathbf{E}} = -x^{\mathbf{B}}\cos\theta + z^{\mathbf{B}}\sin\theta \end{cases}. \tag{A.2}$$

## Appendix B: $\mathbf{v}^{\mathbf{B}}(t)$ in the B-fixed system

Let the initial electron velocity at $t=0$ be $\mathbf{v}^{\mathbf{B}}(0) = \mathbf{v}_0^{\mathbf{B}} = (v_{x0}^{\mathbf{B}}, v_{y0}^{\mathbf{B}}, v_{z0}^{\mathbf{B}})$. In non-ECR condition $\omega_E \neq \omega_B$, an analytic solution of (5) for $\mathbf{v}^{\mathbf{B}}(t)$ is

$$\begin{aligned} v_x^{\mathbf{B}} = &\left(-\frac{\omega_E^2}{\omega_E^2-\omega_B^2}v_E\sin\theta\cos\phi + v_{x0}^{\mathbf{B}}\right)\cos\omega_B t \\ &+\left(+\frac{\omega_E\omega_B}{\omega_E^2-\omega_B^2}v_E\sin\theta\sin\phi - v_{y0}^{\mathbf{B}}\right)\sin\omega_B t \\ &+\frac{\omega_E^2}{\omega_E^2-\omega_B^2}v_E\sin\theta\cos(\omega_E t+\phi), \end{aligned} \tag{B.3}$$

$$\begin{aligned} v_y^{\mathbf{B}} = &\left(-\frac{\omega_E^2}{\omega_E^2-\omega_B^2}v_E\sin\theta\cos\phi + v_{x0}^{\mathbf{B}}\right)\sin\omega_B t \\ &+\left(-\frac{\omega_E\omega_B}{\omega_E^2-\omega_B^2}v_E\sin\theta\sin\phi + v_{y0}^{\mathbf{B}}\right)\cos\omega_B t \\ &+\frac{\omega_E\omega_B}{\omega_E^2-\omega_B^2}v_E\sin\theta\sin(\omega_E t+\phi), \end{aligned} \tag{B.4}$$

$$v_z^{\mathbf{B}} = v_E\cos\theta\cos(\omega_E t+\phi) - v_E\cos\theta\cos\phi + v_{z0}^{\mathbf{B}}. \tag{B.5}$$

In the ECR condition $\omega_E = \omega_B \equiv \omega$,

$$\begin{aligned} v_x^{\mathbf{B}} = &\left(-\frac{1}{2}v_E\sin\theta\sin\phi\cos\phi - \frac{1}{2}\omega t v_E\sin\theta\right. \\ &\left.+ v_{x0}^{\mathbf{B}}\sin\phi - v_{y0}^{\mathbf{B}}\cos\phi\right)\sin(\omega t+\phi) \\ &+\left(+\frac{1}{2}v_E\sin\theta\sin^2\phi + v_{x0}^{\mathbf{B}}\cos\phi + v_{y0}^{\mathbf{B}}\sin\phi\right) \\ &\times\cos(\omega t+\phi), \end{aligned} \tag{B.6}$$

$$\begin{aligned} v_y^{\mathbf{B}} = &\left(+\frac{1}{2}v_E\sin\theta\sin\phi\cos\phi + \frac{1}{2}\omega t v_E\sin\theta\right. \\ &\left.- v_{x0}^{\mathbf{B}}\sin\phi + v_{y0}^{\mathbf{B}}\cos\phi\right)\cos(\omega t+\phi) \\ &+\left(-\frac{1}{2}v_E\sin\theta\cos^2\phi + v_{x0}^{\mathbf{B}}\cos\phi + v_{y0}^{\mathbf{B}}\sin\phi\right) \\ &\times\sin(\omega t+\phi), \end{aligned} \tag{B.7}$$

$$v_z^{\mathbf{B}} = v_E\cos\theta\cos(\omega t+\phi) - v_E\cos\theta\cos\phi + v_{z0}^{\mathbf{B}}. \tag{B.8}$$

## Appendix C: $\mathbf{v}^{\mathbf{E}}(t)$ in the E-fixed system

With $\mathbf{v}^{\mathbf{E}}(0) = \mathbf{v}_0^{\mathbf{E}} = (v_{x0}^{\mathbf{E}}, v_{y0}^{\mathbf{E}}, v_{z0}^{\mathbf{E}})$, analytic solution of (5) for $\mathbf{v}^{\mathbf{E}}(t)$ in the non-ECR condition $\omega_E \neq \omega_B$ is

$$\begin{aligned} v_x^{\mathbf{E}} = &\left(-\frac{\omega_E^2}{\omega_E^2-\omega_B^2}v_E\sin^2\theta\cos\phi\right. \\ &\left.+ v_{x0}^{\mathbf{E}}\sin^2\theta - v_{z0}^{\mathbf{E}}\sin\theta\cos\theta\right)\cos\omega_B t \\ &+\left(+\frac{\omega_E\omega_B}{\omega_E^2-\omega_B^2}v_E\sin^2\theta\sin\phi - v_{y0}^{\mathbf{E}}\sin\theta\right) \\ &\times\sin\omega_B t \\ &+\left(1+\frac{\omega_B^2}{\omega_E^2-\omega_B^2}\sin^2\theta\right)v_E\cos(\omega_E t+\phi) \\ &-v_E\cos^2\theta\cos\phi + v_{x0}^{\mathbf{E}}\cos^2\theta + v_{z0}^{\mathbf{E}}\sin\theta\cos\theta, \end{aligned} \tag{C.9}$$

$$\begin{aligned} v_y^{\mathbf{E}} = &\left(-\frac{\omega_E^2}{\omega_E^2-\omega_B^2}v_E\sin\theta\cos\phi + v_{x0}^{\mathbf{E}}\sin\theta - v_{z0}^{\mathbf{E}}\cos\theta\right) \\ &\times\sin\omega_B t \\ &+\left(-\frac{\omega_E\omega_B}{\omega_E^2-\omega_B^2}v_E\sin\theta\sin\phi + v_{y0}^{\mathbf{E}}\right)\cos\omega_B t \\ &+\frac{\omega_E\omega_B}{\omega_E^2-\omega_B^2}v_E\sin\theta\sin(\omega_E t+\phi), \end{aligned} \tag{C.10}$$

$$\begin{aligned} v_z^{\mathbf{E}} = &\left(+\frac{\omega_E^2}{\omega_E^2-\omega_B^2}v_E\sin\theta\cos\theta\cos\phi\right. \\ &\left.- v_{x0}^{\mathbf{E}}\sin\theta\cos\theta + v_{z0}^{\mathbf{E}}\cos^2\theta\right)\cos\omega_B t \\ &+\left(-\frac{\omega_E\omega_B}{\omega_E^2-\omega_B^2}v_E\sin\theta\cos\theta\sin\phi + v_{y0}^{\mathbf{E}}\cos\theta\right) \\ &\times\sin\omega_B t \\ &-\frac{\omega_B^2}{\omega_E^2-\omega_B^2}v_E\sin\theta\cos\theta\cos(\omega_E t+\phi) \\ &-v_E\sin\theta\cos\theta\cos\phi + v_{x0}^{\mathbf{E}}\sin\theta\cos\theta + v_{z0}^{\mathbf{E}}\sin^2\theta. \end{aligned} \tag{C.11}$$

In the ECR condition $\omega_E = \omega_B \equiv \omega$,

$$\begin{aligned} v_x^{\mathbf{E}} = &\left(+v_{x0}^{\mathbf{E}}\sin\theta\cos\phi + v_{y0}^{\mathbf{E}}\sin\phi - v_{z0}^{\mathbf{E}}\cos\theta\cos\phi\right) \\ &\times\sin\theta\cos(\omega t+\phi) \\ &+\frac{1}{2}v_E\left(2\cos^2\theta+\sin^2\theta\sin^2\phi\right)\cos(\omega t+\phi) \\ &+\left(-\frac{1}{2}v_E\sin\theta\sin\phi\cos\phi + v_{x0}^{\mathbf{E}}\sin\theta\sin\phi\right. \\ &\left.- v_{y0}^{\mathbf{E}}\cos\phi - v_{z0}^{\mathbf{E}}\cos\theta\sin\phi\right)\sin\theta\sin(\omega t+\phi) \\ &-\frac{1}{2}\omega t v_E\sin^2\theta\sin(\omega t+\phi) \\ &-v_E\cos^2\theta\cos\phi + v_{x0}^{\mathbf{E}}\cos^2\theta + v_{z0}^{\mathbf{E}}\sin\theta\cos\theta, \end{aligned} \tag{C.12}$$

$$v_y^{\mathbf{E}} = \left(-\frac{1}{2}v_E\sin\theta\cos^2\phi + v_{x0}^{\mathbf{E}}\sin\theta\cos\phi\right.$$

$$+ v_{y0}^{\mathbf{E}} \sin\phi - v_{z0}^{\mathbf{E}} \cos\theta \cos\phi \Big) \sin(\omega t + \phi)$$
$$+ \Big( + \frac{1}{2} v_E \sin\theta \sin\phi \cos\phi - v_{x0}^{\mathbf{E}} \sin\theta \sin\phi$$
$$+ v_{y0}^{\mathbf{E}} \cos\phi + v_{z0}^{\mathbf{E}} \cos\theta \sin\phi \Big) \cos(\omega t + \phi)$$
$$+ \frac{1}{2} \omega t v_E \sin\theta \cos(\omega t + \phi), \tag{C.13}$$

$$v_z^{\mathbf{E}} = \Big( + \frac{1}{2} v_E \sin\theta (1 + \cos^2\phi) - v_{x0}^{\mathbf{E}} \sin\theta \cos\phi$$
$$- v_{y0}^{\mathbf{E}} \sin\phi + v_{z0}^{\mathbf{E}} \cos\theta \cos\phi \Big) \cos\theta \cos(\omega t + \phi)$$
$$+ \Big( + \frac{1}{2} v_E \sin\theta \sin\phi \cos\phi - v_{x0}^{\mathbf{E}} \sin\theta \sin\phi$$
$$+ v_{y0}^{\mathbf{E}} \cos\phi + v_{z0}^{\mathbf{E}} \cos\theta \sin\phi \Big) \cos\theta \sin(\omega t + \phi)$$
$$+ \frac{1}{2} \omega t v_E \sin\theta \cos\theta \sin(\omega t + \phi)$$
$$- v_E \sin\theta \cos\theta \cos\phi + v_{x0}^{\mathbf{E}} \sin\theta \cos\theta + v_{z0}^{\mathbf{E}} \sin^2\theta. \tag{C.14}$$

Both of these ECR and non-ECR solutions are convertible between the **B**-fixed and the **E**-fixed systems with relations (A.1) and (A.2).

## Appendix D: Acceleration acting on electrons in the B-fixed system

In the **B**-fixed system, the equation of motion (5) for an electron becomes

$$\frac{\mathrm{d}}{\mathrm{d}t} v_x^{\mathbf{B}} = -\frac{eB}{m} v_y^{\mathbf{B}} - \frac{eE}{m} \sin\theta \sin(\omega_E t + \phi), \tag{D.15}$$
$$\frac{\mathrm{d}}{\mathrm{d}t} v_y^{\mathbf{B}} = \frac{eB}{m} v_x^{\mathbf{B}}, \tag{D.16}$$
$$\frac{\mathrm{d}}{\mathrm{d}t} v_z^{\mathbf{B}} = -\frac{eE}{m} \cos\theta \sin(\omega_E t + \phi). \tag{D.17}$$

We obtain the following relations:

$$\left( \frac{\mathrm{d}}{\mathrm{d}t} v_x^{\mathbf{B}}, \frac{\mathrm{d}}{\mathrm{d}t} v_y^{\mathbf{B}}, \frac{\mathrm{d}}{\mathrm{d}t} v_z^{\mathbf{B}} \right)$$
$$\cdot \left( v_x^{\mathbf{B}}, v_y^{\mathbf{B}} + \frac{E}{B} \sin\theta \sin(\omega_E t + \phi), 0 \right) = 0, \tag{D.18}$$

$$\sqrt{\left( \frac{\mathrm{d}}{\mathrm{d}t} v_x^{\mathbf{B}} \right)^2 + \left( \frac{\mathrm{d}}{\mathrm{d}t} v_y^{\mathbf{B}} \right)^2}$$
$$= \frac{eB}{m} \sqrt{(v_x^{\mathbf{B}})^2 + \left( v_y^{\mathbf{B}} + \frac{E}{B} \sin\theta \sin(\omega_E t + \phi) \right)^2}. \tag{D.19}$$

Equation (D.18), which gives the inner product between two vectors, represents that the instantaneous acceleration acting on an electron having a velocity $\mathbf{v}^{\mathbf{B}} = (v_x^{\mathbf{B}}, v_y^{\mathbf{B}}, v_z^{\mathbf{B}})$ is always perpendicular to its position vector relative to a point $(0, -(E/B)\sin\theta\sin(\omega_E t + \phi), v_z^{\mathbf{B}})$. This point is on a central axis of rotation $C$ represented as $v_x = 0$ and $v_y = -(E/B)\sin\theta\sin(\omega_E t + \phi)$. $C$ is parallel to the $v_z$-axis, and moves temporally up and down across the origin $O$ of velocity space (see Fig. 5). Equation (D.19) represents that the acceleration is proportional to the distance of $\mathbf{v}^{\mathbf{B}}$ from $C$ and that the angular frequency $\omega_B = eB/m$ of the rotation is constant irrespective of $\mathbf{v}^{\mathbf{B}}$. The acceleration for $v_z^{\mathbf{B}}$ induces a translational shift along the $v_z$-axis (i.e. along $C$) in velocity space because $\mathrm{d}v_z^{\mathbf{B}}/\mathrm{d}t$ is equal for all electrons.

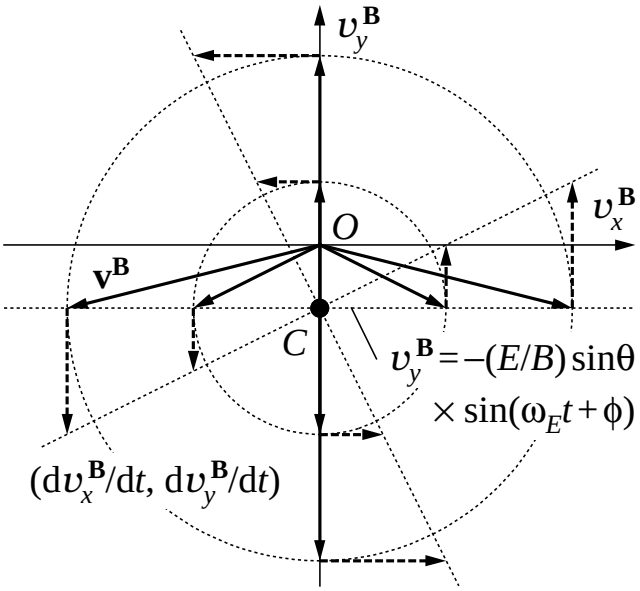


**Fig. 5** Schematic of electron acceleration under $\mathbf{E}(t) = (E\sin\theta\sin(\omega_E t + \phi), 0, E\cos\theta\sin(\omega_E t + \phi))$ and $\mathbf{B} = (0, 0, B)$ projected to the $v_x^{\mathbf{B}} v_y^{\mathbf{B}}$-plane in velocity space. The instantaneous direction of acceleration $(\mathrm{d}v_x^{\mathbf{B}}/\mathrm{d}t, \mathrm{d}v_y^{\mathbf{B}}/\mathrm{d}t)$ (broken arrows) acting on electrons with velocity $\mathbf{v}^{\mathbf{B}}$ (thick arrows) is rotational around a central axis $C$: $(v_x^{\mathbf{B}}, v_y^{\mathbf{B}}) = (0, -(E/B)\sin\theta\sin(\omega_E t + \phi))$ (full circle)

In consequence, the infinitesimal motion of the electrons in velocity space by the instantaneous acceleration is helical; i.e. a composition of the rotation around $C$ and the parallel shift along $C$. The shape of the EVDF of an electron swarm subset remains isotropic around its center in this acceleration.

## Appendix E: Details on electron collision cross sections of CCF model gas

The CCF model gas used for the Monte Carlo simulations has the following electron collision cross sections [55], where $q_{\mathrm{el}}$ is for elastic collision, $q_{\mathrm{inel},1}$ and $q_{\mathrm{inel},2}$ are for inelastic collisions with loss energies of 10 and

15 eV, respectively, and $\varepsilon_{1\mathrm{eV}} = 1\,\mathrm{eV}$:

$$q_{\mathrm{total}}(\varepsilon) = q_0/\sqrt{\varepsilon/\varepsilon_{1\mathrm{eV}}}, \tag{E.20}$$

$$q_0 = 4.0 \times 10^{-19}\,\mathrm{m}^2, \tag{E.21}$$

$$q_{\mathrm{inel},1}(\varepsilon) = \begin{cases} 0 \text{ for } \varepsilon \le 10\,\mathrm{eV} \\ q_1[1-\exp(-0.25\times\varepsilon/\varepsilon_{1\mathrm{eV}})]^{10} \\ \quad \times \exp[-0.01712\times(\varepsilon/\varepsilon_{1\mathrm{eV}} - 10)] \\ \quad \text{for } 10\,\mathrm{eV} < \varepsilon \le 300\,\mathrm{eV} \\ q_1 \exp[-0.01712\times(\varepsilon/\varepsilon_{1\mathrm{eV}} - 10)] \\ \quad \text{for } \varepsilon > 300\,\mathrm{eV} \end{cases}, \tag{E.22}$$

$$q_1 = 1.5 \times 10^{-20}\,\mathrm{m}^2, \tag{E.23}$$

$$q_{\mathrm{inel},2}(\varepsilon) = \begin{cases} 0 \text{ for } \varepsilon \le 15\,\mathrm{eV} \\ q_2\{1-\exp[-(\varepsilon/\varepsilon_{1\mathrm{eV}})^{0.1}]\}^6 \\ \quad \times \exp[-0.0015\times(\varepsilon/\varepsilon_{1\mathrm{eV}} - 15)] \\ \quad \text{for } 15\,\mathrm{eV} < \varepsilon \le 500\,\mathrm{eV} \\ q_2 \exp[-0.0015\times(\varepsilon/\varepsilon_{1\mathrm{eV}} - 15)] \\ \quad \text{for } \varepsilon > 500\,\mathrm{eV} \end{cases}, \tag{E.24}$$

$$q_2 = 2.0 \times 10^{-20}\,\mathrm{m}^2, \tag{E.25}$$

$$q_{\mathrm{el}}(\varepsilon) = q_{\mathrm{total}}(\varepsilon) - q_{\mathrm{inel},1}(\varepsilon) - q_{\mathrm{inel},2}(\varepsilon). \tag{E.26}$$

The original $q_{\mathrm{inel},2}$ [55] is an ionization cross section, but it is treated as an excitation cross section in this work when the electron-conservative case is examined. In the demonstration of the electron-nonconservative case, $q_{\mathrm{inel},2}$ is restored to be the ionization cross section. The residual energy after the production of a secondary electron by a primary electron is divided into two portions to be assigned to the two electrons at a ratio $\delta : (1-\delta)$ with an energy division ratio $\delta$, and $\delta$ is assumed to be equiprobable in a range $0 \le \delta \le 1$.

## Appendix F: Semi-major axis and vertices of elliptic vector locus

The calculation of the vector length $L = |\mathbf{W}(t)|$ can be rearranged into the following form:

$$L^2 = [W_x(t)]^2 + [W_y(t)]^2 + [W_z(t)]^2 \tag{F.27}$$

$$= P\cos^2\alpha + Q\cos\alpha\sin\alpha + R\sin^2\alpha \tag{F.28}$$

$$= \frac{P+R}{2} + \frac{Q}{2}\sin 2\alpha + \frac{P-R}{2}\cos 2\alpha \tag{F.29}$$

$$= \frac{P+R}{2} + \frac{\sqrt{Q^2+(P-R)^2}}{2}\sin(2\alpha+\beta), \tag{F.30}$$

where

$$P = v_E^2\omega_E^2\left[\frac{\omega_E^2\sin^2\theta}{\Omega} + \frac{\omega_E^2\cos^2\theta}{\Xi^2}\right], \tag{F.31}$$

$$Q = -2v_E^2\omega_E^2\left[\frac{\nu\omega_E\sin^2\theta}{\Omega} + \frac{\nu\omega_E\cos^2\theta}{\Xi^2}\right], \tag{F.32}$$

$$R = v_E^2\omega_E^2\left[\frac{(\omega_B^2+\nu^2)\sin^2\theta}{\Omega} + \frac{\nu^2\cos^2\theta}{\Xi^2}\right], \tag{F.33}$$

$$\Omega = \left[(\omega_E-\omega_B)^2+\nu^2\right]\left[(\omega_E+\omega_B)^2+\nu^2\right], \tag{F.34}$$

$$\Xi = \omega_E^2 + \nu^2, \tag{F.35}$$

$$\alpha = \omega_E t + \phi, \tag{F.36}$$

$$(\cos\beta, \sin\beta) = \left(\frac{Q}{\sqrt{Q^2+(P-R)^2}}, \frac{P-R}{\sqrt{Q^2+(P-R)^2}}\right). \tag{F.37}$$

$L^2$ can be rewritten as

$$L^2 = \frac{1}{2}v_E^2\omega_E^2\left[\frac{(\omega_E^2+\omega_B^2+\nu^2)\sin^2\theta}{\Omega} + \frac{\cos^2\theta}{\Xi}\right] + \frac{1}{2}v_E^2\omega_E^2\sqrt{\frac{\sin^2\theta}{\Omega} - \frac{\omega_B^4\sin^2\theta\cos^2\theta}{\Omega\Xi^2} + \frac{\cos^2\theta}{\Xi^2}} \times \sin(2\alpha+\beta). \tag{F.38}$$

$L$ becomes its maximum (i.e. the length of the semi-major axis of the elliptic vector locus) when $\sin(2\alpha+\beta) = 1$ twice in a domain $0 \le \alpha < 2\pi$, and $\mathbf{W}(t)$ points the vertices of the ellipse at that time. Such $\mathbf{W}(t)$ is specified by (14)–(16) with the $\sin\alpha$ and $\cos\alpha$ values corresponding to $\alpha = \pi/4 - \beta/2$ and $5\pi/4 - \beta/2$:

$$\sin\alpha = \pm\frac{\sqrt{2}}{2}\cos\frac{\beta}{2} \mp \frac{\sqrt{2}}{2}\sin\frac{\beta}{2} = \pm\frac{1}{2}\sqrt{1+\cos\beta} \mp \frac{1}{2}\sqrt{1-\cos\beta}, \tag{F.39}$$

$$\cos\alpha = \pm\frac{\sqrt{2}}{2}\cos\frac{\beta}{2} \pm \frac{\sqrt{2}}{2}\sin\frac{\beta}{2} = \pm\frac{1}{2}\sqrt{1+\cos\beta} \pm \frac{1}{2}\sqrt{1-\cos\beta}. \tag{F.40}$$

$X$ in (25) is $\cos\beta$ in (F.37) calculated with $P$, $Q$, and $R$ in (F.31)–(F.33).

## Author contribution statement

H. S. organized this work, derived the theoretical formulae, performed computations, and wrote the manuscript. Y. N. participated in verifying the formulae and editing the manuscript. Both authors discussed the results and contributed to the final article.

## References


1. O. Tarvainen, S.X. Peng, New J. Phys. **18**, 105008 (2016). doi: 10.1088/1367-2630/18/10/105008
2. N. Hayashi, T. Nakashima, H. Fujita, Jpn. J. Appl. Phys. **38**, 4301 (1999). doi: 10.1143/JJAP.38.4301
3. T.A. Santhosh Kumar, S.K. Mattoo, R. Jha, Phys. Plasmas **11**, 1735 (2004). doi: 10.1063/1.1669391
4. St. Kolev, St. Lishev, A. Shivarova, Kh. Tarnev, R. Wilhelm, Plasma Phys. Control. Fusion **49**, 1349 (2007). doi: 10.1088/0741-3335/49/9/001
5. A. Aanesland, J. Bredin, P. Chabert, V. Godyak, Appl. Phys. Lett. **100**, 044102 (2012). doi: 10.1063/1.3680088

6. S.K. Singh, P.K. Srivastava, L.M. Awasthi, S.K. Mattoo, A.K. Sanyasi, R. Singh, P.K. Kaw, Rev. Sci. Instrum. **85**, 033507 (2014). doi: 10.1063/1.4868514
7. G. Fubiani, J.P. Boeuf, Plasma Sources Sci. Technol. **24**, 055001 (2015). doi: 10.1088/0963-0252/24/5/055001
8. J.Y. Kim, W.-H. Cho, J.-J. Dang, S. Kim, Plasma Sources Sci. Technol. **25**, 065019 (2016). doi: 10.1088/0963-0252/25/6/065019
9. J.Y. Kim, W.-H. Cho, J.-J. Dang, K.-J. Chung, Y.S. Hwang, Rev. Sci. Instrum. **87**, 02B117 (2016). doi: 10.1063/1.4933090
10. O. Fukumasa, Y. Tauchi, S. Sakiyama, Jpn. J. Appl. Phys. **36**, 4593 (1997). doi: 10.1143/JJAP.36.4593
11. M. Vural, R.P. Brinkmann, J. Phys. D: Appl. Phys. **40**, 510 (2007). doi:10.1088/0022-3727/40/2/027
12. T. Uchida, Jpn. J. Appl. Phys. **33**, L43 (1994). doi: 10.1143/JJAP.33.L43
13. H. Tsuboi, M. Itoh, M. Tanabe, T. Hayashi, T. Uchida, Jpn. J. Appl. Phys. **34**, 2476 (1995). doi: 10.1143/JJAP.34.2476
14. H. Asakura, K. Takemura, Z. Yoshida, and T. Uchida, Jpn. J. Appl. Phys. **36**, 4493 (1997). doi: 10.1143/JJAP.36.4493
15. T. Uchida, J. Vac. Sci. Technol. A **16**, 1529 (1998). doi: 10.1116/1.581182
16. W. Chen, M. Ito, T. Hayashi, T. Uchida, J. Vac. Sci. Technol. A **16**, 1594 (1998). doi: 10.1116/1.581193
17. H. Sugawara, S. Ogino, Jpn. J. Appl. Phys. **55**, 07LD05 (2016). doi: 10.7567/JJAP.55.07LD05
18. M. Tadokoro, H. Hirata, N. Nakano, Z.Lj. Petrović, T. Makabe, Phys. Rev. E **57**, R43 (1998). doi: 10.1103/PhysRevE.57.R43
19. A.V. Vasenkov, M.J. Kushner, J. Appl. Phys. **94**, 5522 (2003). doi: 10.1063/1.1614428
20. H. Takahashi, H. Sugawara, Jpn. J. Appl. Phys. **59**, 036001 (2020). doi: 10.35848/1347-4065/ab71d2
21. T. Uchida, S. Hamaguchi, J. Phys. D: Appl. Phys. **41**, 083001 (2008). doi: 10.1088/0022-3727/41/8/083001
22. Z.Lj. Petrović, S. Dujko, D. Marić, G. Malović, Ž. Nikitović, O. Šašić, J. Jovanović, V. Stojanović, M. Radmilović-Rađenović, J. Phys. D: Appl. Phys. **42**, 194002 (2009). doi: 10.1088/0022-3727/42/19/194002
23. I. Adamovich *et al.*, J. Phys. D: Appl. Phys. **50** 323001 (2017). doi: 10.1088/1361-6463/aa76f5
24. A. Bogaerts, E. Bultinck, I. Kolev, L. Schwaederlé, K. Van Aeken, G. Buyle, D. Depla, J. Phys. D: Appl. Phys., **42**, 194018 (2009). doi: 10.1088/0022-3727/42/19/194018
25. K. Kamimura, K. Iyanagi, N. Nakano, T. Makabe, Jpn. J. Appl. Phys. **38**, 4429 (1999). doi: 10.1143/JJAP.38.4429
26. G.R. Govinda Raju, M.S. Dincer, IEEE Trans. Plasma Sci. **18**, 819 (1990). doi: 10.1109/27.62348
27. M.S. Dincer and A. Gokmen, J. Phys. D: Appl. Phys. **25**, 942 (1992). doi: 10.1088/0022-3727/25/6/007
28. M.S. Dincer, J. Phys. D: Appl. Phys. **26**, 1427 (1993). doi: 10.1088/0022-3727/26/9/013
29. N. Shimura, T. Makabe, Appl. Phys. Lett. **62**, 678 (1993). doi: 10.1063/1.108837
30. K.F. Ness, Phys. Rev. E **47** 327 (1993). doi: 10.1103/PhysRevE.47.327
31. K.F. Ness, J. Phys. D: Appl. Phys. **27**, 1848 (1994). doi: 10.1088/0022-3727/27/9/007
32. B. Li, R.D. White, R.E. Robson, K.F. Ness, Annals Phys. **292**, 179 (2001). doi: 10.1006/aphy.2001.6171
33. R.D. White, K.F. Ness, R.E. Robson, J. Phys. D: Appl. Phys. **32**, 1842 (1999). doi: 10.1088/0022-3727/32/15/312
34. R.D. White, K.F. Ness, R.E. Robson, B. Li, Phys. Rev. E **60**, 2231 (1999). doi: 10.1103/PhysRevE.60.2231
35. R.D. White, R.E. Robson, K.F. Ness, J. Phys. D: Appl. Phys. **34**, 2205 (2001). doi: 10.1088/0022-3727/34/14/316
36. R.D. White, R.E. Robson, K.F. Ness, T. Makabe, J. Phys. D: Appl. Phys. **38**, 997 (2005). doi: 10.1088/0022-3727/38/7/006
37. S. Dujko, R.D. White, K.F. Ness, Z.Lj. Petrović, R.E. Robson, J. Phys. D: Appl. Phys. **39**, 4788 (2006). doi: 10.1088/0022-3727/39/22/009
38. S. Dujko, R.D. White, Z.Lj. Petrović, R.E. Robson, Phys. Rev. E **81**, 046403 (2010). doi: 10.1103/PhysRevE.81.046403
39. S. Dujko, R.D. White, Z.Lj. Petrović, R.E. Robson, Plasma Sources Sci. Technol. **20**, 024013 (2011). doi: 10.1088/0963-0252/20/2/024013
40. R.D. White, K.F. Ness, R.E. Robson, Appl. Surf. Sci., **192**, 26 (2002). doi: 10.1016/S0169-4332(02)00019-3
41. Z.M. Raspopović, S. Dujko, T. Makabe, Z.Lj. Petrović, Plasma Sources Sci. Technol. **14**, 293 (2005). doi: 10.1088/0963-0252/14/2/010
42. O. Šašić, S. Dujko, Z.Lj. Petrović, T. Makabe, Jpn. J. Appl. Phys. **46**, 3560 (2007). doi: 10.1143/JJAP.46.3560
43. R.D. White, S. Dujko, K.F. Ness, R.E. Robson, Z. Raspopović, Z.Lj. Petrović, J. Phys. D: Appl. Phys. **41** 025206 (2008). doi: 10.1088/0022-3727/41/2/025206
44. S. Dujko, D. Bošnjaković, R.D. White, Z.Lj. Petrovicć, Plasma Sources Sci. Technol. **24**, 054006 (2015). doi: 10.1088/0963-0252/24/5/054006
45. S. Dujko, R.D. White, Z.Lj. Petrovicć, IEEE Trans. Plasma Sci. **39**, 2560 (2011). doi: 10.1109/TPS.2011.2150246
46. Y. Nakamura, M. Kurachi, J. Phys. D: Appl. Phys. **21**,718 (1988). doi: 10.1088/0022-3727/21/5/008
47. T. Sato, H. Sugawara, *Proceedings of XXXIV International Conference on Phenomena in Ionized Gases, 10th International Conference on Reactive Plasmas, 37th Symposium on Plasma Processing, and 32nd Symposium on Plasma Science for Materials, Sapporo, Japan, 2019*, PO18AM-003
48. H. Sugawara, Jpn. J. Appl. Phys. **58**, 108002 (2019). doi: 10.7567/1347-4065/ab3e5d
49. H. Sugawara, *Bulletin of the American Physical Society, 72nd Annual Gaseous Electronics Conference, College Station, Texas, USA, 2019*, FT1.00064
50. H. Sugawara, T. Yahata, A. Oda, Y. Sakai, J. Phys. D: Appl. Phys., **33**, 1191 (2000). doi: 10.1088/0022-3727/33/10/309
51. Y. Nakata, T. Sato, H. Sugawara, IEEE Trans. Plasma Sci. **49**, 83 (2021). doi: 10.1109/TPS.2020.3010315
52. M. Hayashi, S. Ushiroda, J. Chem. Phys. **78**, 2621 (1983). doi: 10.1063/1.445019
53. M. Hayashi, T. Nimura, J. Appl. Phys. **54**, 4879 (1983). doi: 10.1063/1.332797
54. H. Sugawara, Y. Nakata, *Book of Abstracts POSMOL 2021 at-present: XXII International Symposium on Electron-Molecule Collisions and Swarms, The University of Notre Dame, Indiana, USA, 2021*, p. 73, No. 41. https://sites.nd.edu/posmol2021conference/
55. K. Satoh, Y. Ohmori, Y. Sakai, H. Tagashira, Trans. IEE Japan A **111**, 198 (1991) doi: 10.1541/ieejfms1990.111.3_198 [in Japanese]